# Ni(II) Phenoxyiminato Olefin Polymerization Catalysis: Striking Coordinative Modulation of Hyperbranched Polymer Microstructure and Stability by a Proximate Sulfonyl Group

**ARTICLE** *in* ACS CATALYSIS · FEBRUARY 2014

Impact Factor: 9.31 · DOI: 10.1021/cs500114b

ACS Catalysis

Letter

pubs.acs.org/acscatalysis

# Ni(II) Phenoxyiminato Olefin Polymerization Catalysis: Striking Coordinative Modulation of Hyperbranched Polymer Microstructure and Stability by a Proximate Sulfonyl Group

Casey J. Stephenson,[†,§] Jennifer P. McInnis,[†,§] Changle Chen,[†] Michael P. Weberski, Jr.,[†] Alessandro Motta,[‡] Massimiliano Delferro,*[,†] and Tobin J. Marks*[,†]

[†]Department of Chemistry, Northwestern University, Evanston, Illinois 60208-3113, United States

[‡]Dipartimento di Scienze Chimiche, Università di Catania and INSTM, UdR Catania, 95125 Catania, Italy

Supporting Information

**ABSTRACT:** The synthesis, structural characterization, and ethylene polymerization properties of two neutrally charged Ni(II) phenoxyiminato catalysts are compared and contrasted. Complex FI-$SO_2$-Ni features a $-SO_2-$ group embedded in the ligand skeleton, whereas control FI-$CH_2$-Ni has the $-SO_2-$ replaced by a $-CH_2-$ functionality. In comparison with FI-$CH_2$-Ni, at 25 °C, FI-$SO_2$-Ni is 18 times more active, produces polyethylene with 3.2 times greater $M_W$ and 1.5 times branch content, and is significantly more thermally stable. The FI-$SO_2$-Ni-derived polymer is a hyperbranched polyethylene (148 branches 1000 $C^{-1}$, $M_W$ = 3500$g$ $mol^{-1}$) versus that from FI-$CH_2$-Ni (98 branches 1000 $C^{-1}$, $M_W$ = 1100$g$ $mol^{-1}$). DFT calculations argue that the distinctive FI-$SO_2$-Ni catalytic behavior versus that of FI-$CH_2$-Ni is associated with nonnegligible OSO···Ni interactions involving the activated catalyst.

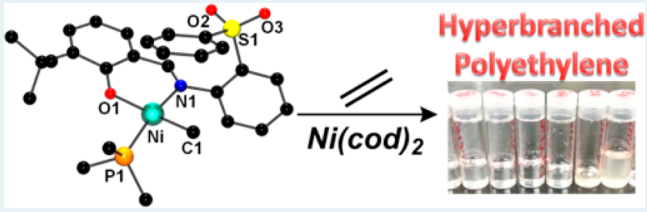


**KEYWORDS:** *hemilabile ligand, sulfonyl group, nickel, hyperbranched polyethylene, DFT calculations*

Late transition metal olefin polymerization catalysts[1] have garnered much attention since the discovery of cationic Ni(II)- and Pd(II)-based $\alpha$-diimine catalysts by Brookhart[2] and neutral Ni(II) phenoxyiminato catalysts by Grubbs.[3] Under ethylene homopolymerization conditions, these catalysts yield polyethylenes that range from linear to highly branched, while also enchaining polar comonomers, stimulating detailed synthetic and mechanistic studies.[3−5] Following olefin insertion, 14-electron intermediates are formed that can undergo either ethylene binding and continued chain propagation or $\beta$-H elimination, which then promotes branch introduction, chain transfer, or catalyst deactivation. In the latter, $\beta$-H elimination leads to formation of a transient Ni−H species, which reductively eliminate to yield metallic Ni and the free ligand.[1b,5] The stabilization of reactive Ni−H species might thereby increase catalyst lifetimes and facilitate chain walking, which in turn could have profound effects on the polymer microstructure.

Hemilabile ligands have been successful in transition metal-mediated catalysis in stabilizing coordinatively unsaturated reactive intermediates via proximate, flexible, weakly coordinating ligands;[6−8] however, such groups in transition metal-mediated olefin polymerization catalysis have been only minimally explored.[9,10] To this end, we report that introducing spatially proximate but electronically remote "hard" $-SO_2-$ groups in the vicinity of "soft" $d^{10}$ catalytic centers offers a new means to modulate single-site polymerization processes (Chart 1).

**Chart 1. (A) General Representation of Stabilization of Coordinatively Unsaturated Reactive Intermediates in Transition Metal Olefin Polymerization Catalysts and (B) Ni(II)phenoxyiminato Catalyst with a Remote $-SO_2-$ Group in the Ligand Framework**

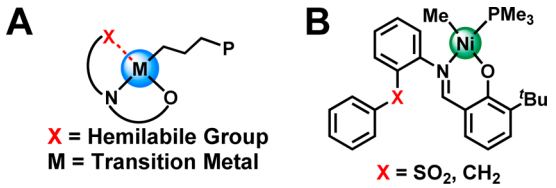


Here we report that a Ni(II)phenoxyiminato catalyst containing a remote ligand $-SO_2-$ group exhibits greatly enhanced olefin polymerization activity and thermal stability and produces higher $M_W$ polyethylenes with remarkably high levels of chain branching (Chart 1, B) versus a $-CH_2-$ control. Hyperbranched polyethylenes are of interest as blending additives in polymer extrusion and as lubricant shear-stable viscosity additives. The performance of such additives should be further enhanced by lowering the $M_W$, increasing short chain branch densities, or both.[11]

Received: January 24, 2014
Revised: January 27, 2014
Published: January 31, 2014

   dx.doi.org/10.1021/cs500114b | ACS Catal. 2014, 4, 999−1003

The catalyst ligands are synthesized by condensing the corresponding anilines with 1.2 equiv of 3-*tert*-butyl-2-hydroxyl benzaldehyde using a catalytic amount of formic acid (Scheme 1). The reactions proceed in high yield and afford products of high purity, as confirmed by conventional spectroscopic and analytical techniques.[12] The ligands are then converted to sodium salts by stirring with excess NaH in THF and were used without further purification (Scheme 1). Metalated precatalysts FI-$SO_2$-Ni and FI-$CH_2$-Ni were then prepared by reacting the respective sodium salts with 1.0 equiv of $NiClMe(PMe_3)_2$ in benzene and were isolated by filtration, followed by removal of the volatiles in vacuo and recrystallization from *n*-hexane (84% and 88% yield, respectively). Diffraction quality crystals were grown from *n*-hexane; the molecular structures are shown in Scheme 1. FI-$SO_2$-Ni and FI-$CH_2$-Ni were characterized by standard spectroscopic and analytical techniques,[12] and the results are in good agreement with the diffraction data. The geometrical parameters of FI-$SO_2$-Ni and FI-$CH_2$-Ni are similar to those of previously reported square−planar Ni(II) phenoxyiminato complexes with the Ni-$PMe_3$ ligand trans to the imine functionality (Scheme 1).[15] Both diamagnetic complexes have distorted square−planar coordination geometries, with P1 and C1 of FI-$SO_2$-Ni and FI-$CH_2$-Ni displaced from the mean O1/Ni1/N1 planes by 0.496 and 0.344 Å and by 0.315 and 0.361 Å, respectively. In the solid state, the O atoms of the FI-$SO_2$-Ni sulfonyl group are orientated *away* from the Ni center (Scheme 1). The $^1H-^1H$ 2D NOESY NMR spectra of FI-$SO_2$-Ni and FI-$CH_2$-Ni display NOE interactions between the *t*-Bu group and the $PMe_3$ ligand, the Ni-$CH_3$ group and the Ni-$PMe_3$ ligand, and the Ni-$CH_3$ group and an aryl-H. This is consistent with the distorted square−planar coordination geometry found in the solid state (Supporting Information (SI) Figures S9 and S10). However, as evidenced by a bis-chelated (FI-$SO_2$-Ph)$_2$Ni side product (see SI Figure S25), the $-SO_2-$ group can coordinate to a similar Ni(II) center and under polymerization conditions should be able to closely approach the Ni(II) center of FI-$SO_2$-Ni (vide infra). In FI-$CH_2$-Ni, a long Ni···H−C(benzyl) contact is observed at 2.56 Å.

**Scheme 1. Synthesis of Ligands HFI-$SO_2$-Ph and HFI-$CH_2$-Ph, and Single-Crystal XRD Structures of Precatalysts FI-$SO_2$-Ni and FI-$CH_2$-Ni**[a]

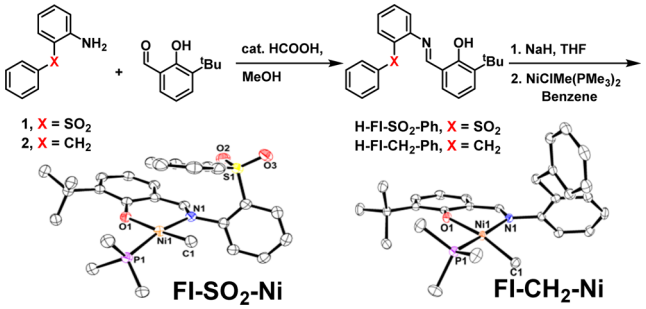


[a]H atoms are omitted for clarity.

Ethylene homopolymerizations were performed using Ni(cod)$_2$ as a phosphine scavenger in toluene at a constant 8 atm ethylene pressure, under conditions minimizing mass transport and exotherm effects (Table 1).[16] A 25 °C, FI-$SO_2$-Ni produces polyethylene with an activity as high as 35 kg of PE mol $[Ni]^{-1}$ $atm^{-1}$ $h^{-1}$ to yield a polymer with $M_W$ = 3500 g $mol^{-1}$ and a polydispersity indicative of single-site behavior. Furthermore, the $^1H$ NMR spectrum of the FI-$SO_2$-Ni-derived polyethylene exhibits 148 branches 1000 $C^{-1}$, which is consistent with extensive chain walking[17] relative to propagation. The unsaturation in the FI-$SO_2$-Ni-derived polyethylene consists of 87% internal olefins (SI Figures S18, S19), which is consistent with $\beta$-H elimination and C=C migration.[17] Under the same conditions, FI-$CH_2$-Ni produces far less polyethylene at an activity of ∼2.2 kg PE mol$[Ni]^{-1}$ $atm^{-1}$ $h^{-1}$, with product $M_W$ = 1100 g $mol^{-1}$ and 98 branches 1000 $C^{-1}$. This latter branch density is comparable to that produced by conventional Ni(II) phenoxyiminato catalysts.[3] It is unlikely that steric effects alone are responsible for the marked FI-$SO_2$-Ni versus FI-$CH_2$-Ni polymerization differences because sterically encumbered ligand substituents tend to suppress $\beta$-H transfer/chain-walking processes in catalysts of this type, yielding nearly linear high-$M_w$ polyethylenes.[1b]

In comparison with FI-$CH_2$-Ni, FI-$SO_2$-Ni is 18 times more active for ethylene polymerization and produces polyethylene that has a 3.2 times higher $M_W$ with 1.5 times greater branch density than does FI-$CH_2$-Ni. $^{13}C$ NMR analysis of the polymer microstructure produced by FI-$SO_2$-Ni at 25 °C reveals a variety of branch types, including methyl, ethyl, *n*-propyl, *n*-butyl, *sec*-butyl, and >C6 (Figure 1), whereas the FI-$CH_2$-Ni product has predominantly methyl and >C6 branches, with a small density of *n*-butyl branches (SI Figures S14 and S15).[13] The presence of *sec*-butyl groups indicates branch-on-branch formation.[1h,13b] The greater branch densities and varied branch architectures introduced by FI-$SO_2$-Ni indicate very rapid chain-walking, likely promoted by sulfonyl group stabilization of 14-electron intermediates (see more below).

**Table 1. Ethylene Polymerization Data for FI-$SO_2$-Ni- and FI-$CH_2$-Ni-Derived Catalysts**[a]

| | | | | | | % branch type[d] | | | | | | | |
|---|---|---|---|---|---|---|---|---|---|---|---|---|---|
| entry | cat. | *T* (°C) | PE (g) | activity[b] | branches (×1000 C)[c] | Me | Et | Pr | Bu[e] | Hex+ | $M_n$ (NMR) (kg/mol)[f] | $M_w$ (GPC) (kg/mol)[g] | PDI[g] |
| 1 | FI-$SO_2$-Ni | 23 | 1.9 | 35 | 148 | 45 | 10 | 4 | 22 | 19 | 2.1 | 3.5 | 1.8 |
| 2 | FI-$CH_2$-Ni | 23 | 0.12 | 2.2 | 98 | 55 | 3 | <1 | 11 | 31 | 0.66 | 1.1 | 1.4 |
| 3 | FI-$SO_2$-Ni | 40 | 2.8 | 53 | 145 | 44 | 9 | 2 | 23 | 22 | 1.6 | 2.8 | 1.9 |
| 4 | FI-$CH_2$-Ni | 40 | trace | | | | | | | | | | |
| 5 | FI-$SO_2$-Ni | 60 | 2.7 | 51 | 150 | 41 | 10 | 3 | 23 | 23 | 1.5 | 2.1 | 1.6 |
| 6 | FI-$CH_2$-Ni | 60 | trace | | | | | | | | | | |

[a]Polymerizations carried out in 25 mL of toluene with 10 $\mu$mol of catalyst at a constant 8.0 atm ethylene pressure for 40 min and using 2 equiv of Ni(cod)$_2$ as phosphine scavenger. All polymerizations were performed in duplicate. [b]kg of PE mol $[Ni]^{-1}$ $atm^{-1}$ $h^{-1}$. [c]By $^1H$ NMR.[13] [d]By $^{13}C$ NMR. [e]Bu = *n*-butyl + *sec*-butyl. [f]By $^1H$ NMR.[14] [g]By GPC vs polystyrene standards.


dx.doi.org/10.1021/cs500114b | ACS Catal. 2014, 4, 999−1003

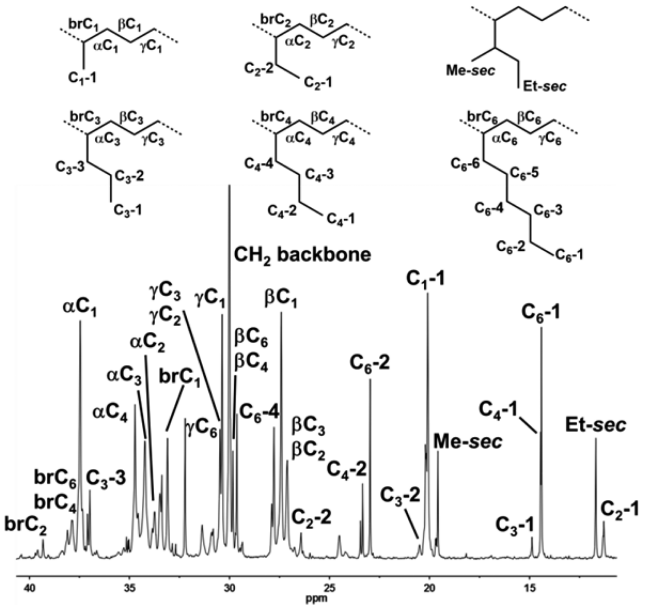


**Figure 1.** 125 MHz $^{13}C\{^1H\}$NMR spectrum of the polyethylene produced by FI-$SO_2$-Ni at 40 °C reaction temperature.

To compare the thermal stability of the catalysts derived from FI-$SO_2$-Ni and FI-$CH_2$-Ni, ethylene polymerizations were performed at elevated temperatures. At 40 °C, activated FI-$CH_2$-Ni rapidly decomposes to yield a black Ni precipitate and negligible quantities of polyethylene (Table 1, entry 4). In contrast, at 40 °C, the catalyst derived from FI-$SO_2$-Ni gives no obvious decomposition over the same reaction time and produces polyethylene at activities slightly higher than at 25 °C (Table 1, entry 3). This result further supports the hypothesis that the sulfonyl group stabilizes the catalyst against deactivation.

The polymer produced by FI-$SO_2$-Ni at 40 °C has $M_W$ = 2800 g $mol^{-1}$ with 145 branches 1000 $C^{-1}$. That the 40 °C branching is similar to that at 25 °C indicates that the chain-walking to propagation rate ratios remain approximately constant over this temperature range. At 60 °C, FI-$SO_2$-Ni polymerization activity remains at 51 kg PE mol[Ni]$^{-1}$ $atm^{-1}$ $h^{-1}$, while the polyethylene $M_W$ has decreased to 2100 g $mol^{-1}$ with the approximately same branch density as at 25 °C. Falling $M_W$ with increased temperature mirrors trends observed in many other single-site catalyst systems,[1g,18] and presumably reflects more favorable $\beta$-H elimination. Furthermore, catalyst activity versus time studies at 60 °C reveal that FI-$SO_2$-Ni undergoes significantly slower decomposition (SI Table S2, Figure S22) than FI-$CH_2$-Ni, which quickly decomposes. Note that the FI-$SO_2$-Ni-derived polymer $M_W$ and branch density are insensitive to polymerization time.

To obtain better insight into the polymerization mechanism, DFT calculations were performed[12] to examine the origin of the catalytic differences between FI-$SO_2$-Ni and FI-$CH_2$-Ni.[19] The geometric, electronic, and energetic properties of all intermediates and transition states in the propagation, branch-forming, and termination pathways were investigated, with the $\gamma$-complex of Scheme 2 taken as the reference point. In addition to the $\gamma$-complex, two other stable structures are identified, related to this structure by rotation of the polymeryl chain.

The first structure involves displacement of the polymer chain agostic interaction by a ligand $SO_2$ or $CH_2$ group of activated FI-$SO_2$-Ni or FI-$CH_2$-Ni, respectively (**PII**). For activated FI-$CH_2$-Ni, **PII** formation is slightly endoergic, whereas it is significantly exoergic for FI-$SO_2$-Ni (Figure 2). This structure precedes ethylene coordination and the subsequent insertion step (propagation pathway, red in Scheme 2). Note that there is no energy barrier for ethylene coordination in FI-$SO_2$-Ni, versus 1.7 kcal $mol^{-1}$ (formation of **PII**) in FI-$CH_2$-Ni (Figure 2). Furthermore, at constant elevated ethylene pressure, the turnover-limiting propagation/insertion step has a slightly lower computed barrier for FI-$SO_2$-Ni ($\Delta G^{\ddagger}_{prop}$ = 14.7 kcal $mol^{-1}$) versus FI-$CH_2$-Ni ($\Delta G^{\ddagger}_{prop}$= 15.2 kcal $mol^{-1}$), in accord with the higher measured polymerization activity of FI-$SO_2$-Ni (Table 1).

**Scheme 2. Proposed Catalytic Cycle for Ethylene Polymerization, Branch Formation, and Catalyst Deactivation Mediated by Activated Catalyst FI-$SO_2$-Ni**

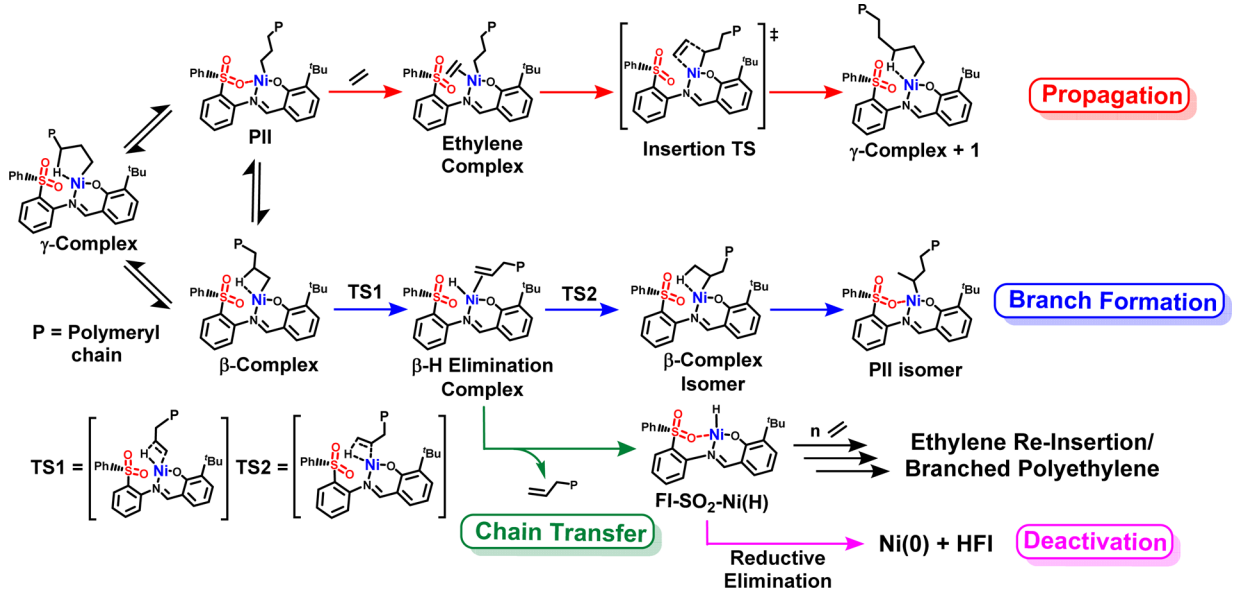



dx.doi.org/10.1021/cs500114b | ACS Catal. 2014, 4, 999−1003

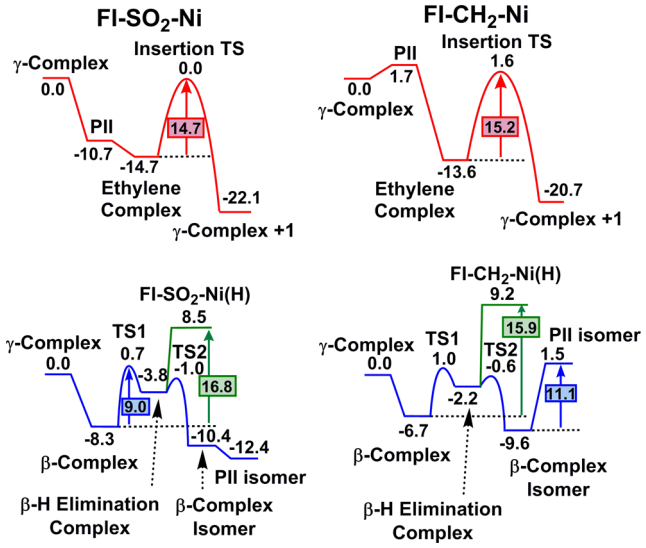


**Figure 2.** Comparative Gibbs free energy profiles (kcal $mol^{-1}$) associated with the propagation (red), branch-forming (blue), and chain transfer (green) pathways for FI-$SO_2$-Ni and FI-$CH_2$-Ni.

The second structure involves a $\beta$-agostic interaction of the growing polymer with the Ni center ($\beta$-complex). For both FI-$SO_2$-Ni and FI-$CH_2$-Ni, $\beta$-agostic formation is exoergic and proceeds with minimal barrier to the $\beta$-H elimination complex, which in turn precedes olefin reinsertion (branch-forming path) or olefin dissociation (chain transfer path). The energetic profiles of the branch-forming pathways (blue in Figure 2) reveal that for FI-$SO_2$-Ni, the activation barrier primarily reflects formation of the $\beta$-H elimination complex ($\Delta G^{\ddagger}_{branc}$ = 9.0 kcal $mol^{-1}$) and, ultimately, the O═S═O···Ni-stabilized **PII** isomer. In contrast, the FI-$CH_2$-Ni barrier reflects $\beta$-agostic interaction dissociation to form the less stable $\beta$-complex and **PII** isomer, necessary for subsequent ethylene coordination ($\Delta G^{\ddagger}_{branc}$ = 11.1 kcal $mol^{-1}$) and propagation of the branched chain. The difference between propagation and branching barriers for FI-$SO_2$-Ni ($\Delta\Delta G^{\ddagger}$ = 5.7 kcal $mol^{-1}$) versus FI-$CH_2$-Ni ($\Delta\Delta G^{\ddagger}$ = 4.1 kcal $mol^{-1}$) shows that branching is slightly more favorable for FI-$SO_2$-Ni, in agreement with experiment. Ethylene insertion at the **PII** isomer, necessary to incorporate the methyl branch into the polymer chain, follows a kinetic trend comparable to that in the propagation step for both the FI-$SO_2$-Ni and FI-$CH_2$-Ni systems (FI-$SO_2$-Ni: $\Delta G^{\ddagger}$prop. isomer = 14.4 kcal $mol^{-1}$; FI-$CH_2$-Ni: $\Delta G^{\ddagger}$ prop. isomer = 14.6 kcal $mol^{-1}$; see Figure S23).

Olefin dissociation from the $\beta$-H elimination structure yields a Ni−H species {FI−Ni(H)} and free polymer (green in Figure 2). The barrier for this chain transfer process is computed as $\Delta G^{\ddagger}_{term}$ = 16.8 kcal $mol^{-1}$ for FI-$SO_2$-Ni, and $\Delta G^{\ddagger}_{term}$ = 15.9 kcal $mol^{-1}$ for FI-$CH_2$-Ni. The greater difference between propagation and chain transfer barriers for FI-$SO_2$-Ni ($\Delta\Delta G^{\ddagger}$ = 2.1 kcal $mol^{-1}$) versus FI-$CH_2$-Ni ($\Delta\Delta G^{\ddagger}$ = 0.7 kcal $mol^{-1}$) is in accord with the higher polyethylene $M_w$ produced by FI-$SO_2$-Ni (Table 1).[19b] Finally, a plausible catalyst deactivation pathway (pink in Scheme 2), at least at high ethylene concentrations, would involve the reductive elimination of the free ligand and Ni(0) from the $\beta$-H elimination/olefin dissociation derived FI−Ni(H).[4b,20] Note that the computed barrier to this first reasonable decomposition step is 1.6 kcal $mol^{-1}$ greater for FI-$SO_2$-Ni than for FI-$CH_2$-Ni,[12] in accord with the increased stability of the FI-$SO_2$-Ni catalyst observed experimentally.

From the forgoing experimental and theoretical discussion, it is evident that the hemilabile $SO_2$ interaction with the metal center in the **PII**, **PII** isomer and FI-$SO_2$-Ni(H) structures can be identified as the primary factor differentiating the reactivities of the two catalysts. For this reason, a more extensive analysis of the electronic structure of species **PII** was carried out. The greater stabilization of **PII** in the activated FI-$SO_2$-Ni vs FI-$CH_2$-Ni catalysts can be ascribed to a monodentate Ni···O═S═O interaction, supported by both geometric and electronic population evidence. An analogous but significantly weaker Ni···H−CH interaction occurs in FI-$CH_2$-Ni. Note that the computed FI-$SO_2$-Ni S−O2 versus S−O1 bond elongation (see SI Figure S24; Δ = +0.042 Å) as well as FI-$CH_2$-Ni Ni···H−C bond elongation (1.187 Å) vs a normal $sp^3$ C−H bond distance of 1.10 Å indicate that secondary interactions occur in both complexes. NBO analysis of **PII** shows that the former elongation is due to partial population of $\sigma^*$ antibonding orbitals localized on the S−O2 and C−H bonds of FI-$SO_2$-Ni and FI-$CH_2$-Ni, respectively. The NBO distribution also reveals stabilizing electron donation from the $SO_2$ or $CH_2$ fragments to the Ni center, with overlap between the lone pair localized on one O atom $sp^2$ orbital and the empty Ni 4s orbital (SI Figure S24). Less efficient electron donation occurs between the $sp^3$ C−H orbital and the FI-$CH_2$-Ni Ni center. These interactions help explain why stabilization by the $SO_2$ group is greater than by the $CH_2$ group in **PII** and FI−Ni(H), and differences in reactivity observed between the FI-$SO_2$-Ni- and FI-$CH_2$-Ni-derived catalysts can be ascribed primarily to this interaction.

In conclusion, these results indicate that a spatially proximate but electronically remote, weakly coordinating ligand −$SO_2$− moiety in a phenoxyiminato-based Ni ethylene polymerization catalyst significantly enhances activity and thermal stability and produces product polymers with exceptional branch densities, indicating that $\beta$-H elimination/olefin reinsertion is especially facile. DFT analysis of the propagation, branch formation, and chain transfer pathways indicates that the proximate $SO_2$ group significantly stabilizes the Ni center relative to the control $CH_2$ complex, explaining the marked differences in FI-$SO_2$-Ni vs FI-$CH_2$-Ni polymerization characteristics. Work is underway to further probe how sulfonyl group sterics and electronics affect catalyst function and product polymer microstructure in other catalysts.

## ■ ASSOCIATED CONTENT

### Supporting Information

Details of ligand and catalyst synthesis and characterization, polymerization experiments, polymer characterization, DFT calculations, and X-ray structures. This material is available free of charge via the Internet at http://pubs.acs.org.

## ■ AUTHOR INFORMATION


### Corresponding Authors

*E-mail: m-delferro@northwestern.edu.

*E-mail: t-marks@northwestern.edu.

### Author Contributions

§C.J.S. and J.P.M. contributed equally to this paper.


### Notes

The authors declare no competing financial interest.

## ■ ACKNOWLEDGMENTS

Financial support by DOE Grant 86ER13511 (M.P.W. and C.C) on the heterogeneous-homogeneous catalytic interface, and by NSF Grant CHE-1213235 (C. J. S. and J. P. M.) on fundamental homogeneous catalysis, is gratefully acknowledged. Use of NMR and X-ray facilities at the IMSERC facility of Northwestern University was supported by NSF under Grants CHE-1048773 and CHE-0923236. We acknowledge CINECA Award N. HP10C9RDDE 2013 for high performance computing resources and support.

## ■ REFERENCES

(1) (a) For recent reviews, see: Nakamura, A.; Anselment, T. M. J.; Claverie, J.; Goodall, B.; Jordan, R. F.; Mecking, S.; Rieger, B.; Sen, A.; van Leeuwen, P. W. N. M.; Nozaki, K. *Acc. Chem. Res.* **2013**, *46*, 1438−1449. (b) Makio, H.; Terao, H.; Iwashita, A.; Fujita, T. *Chem. Rev.* **2011**, *111*, 2363−2449. (c) Delferro, M.; Marks, T. J. *Chem. Rev.* **2011**, *111*, 2450−2485. (d) Gibson, V. C.; Spitzmesser, S. K. *Chem. Rev.* **2002**, *103*, 283−316. (e) Mecking, S. *Coord. Chem. Rev.* **2000**, *203*, 325−351. (f) Ittel, S. D.; Johnson, L. K.; Brookhart, M. *Chem. Rev.* **2000**, *100*, 1169−1204.

(2) Johnson, L. K.; Killian, C. M.; Brookhart, M. *J. Am. Chem. Soc.* **1995**, *117*, 6414−6415.

(3) (a) Waltman, A. W.; Younkin, T. R.; Grubbs, R. H. *Organometallics* **2004**, *23*, 5121−5123. (b) Connor, E. F.; Younkin, T. R.; Henderson, J. I.; Waltman, A. W.; Grubbs, R. H. *Chem. Commun.* **2003**, *18*, 2272−2273. (c) Connor, E. F.; Younkin, T. R.; Henderson, J. I.; Hwang, S.; Grubbs, R. H.; Roberts, W. P.; Litzau, J. J. *J. Polym. Sci. A: Polym. Chem.* **2002**, *40*, 2842−2854. (d) Younkin, T. R.; Connor, E. F.; Henderson, J. I.; Friedrich, S. K.; Grubbs, R. H.; Bansleben, D. A. *Science* **2000**, *287*, 460−462.

(4) (a) Weberski, M. P.; Chen, C.; Delferro, M.; Zuccaccia, C.; Macchioni, A.; Marks, T. J. *Organometallics* **2012**, *31*, 3773−3789. (b) Weberski, M. P.; Chen, C.; Delferro, M.; Marks, T. J. *Chem.—Eur. J.* **2012**, *18*, 10715−10732. (c) Chen, C.; Luo, S.; Jordan, R. F. *J. Am. Chem. Soc.* **2010**, *132*, 5273−5284. (d) Delferro, M.; McInnis, J. P.; Marks, T. J. *Organometallics* **2010**, *29*, 5040−5049. (e) Berkefeld, A.; Möller, H. M.; Mecking, S. *Organometallics* **2009**, *28*, 4048−4055. (f) Berkefeld, A.; Mecking, S. *J. Am. Chem. Soc.* **2009**, *131*, 1565−1574.

(5) Berkefeld, A.; Mecking, S. *J. Am. Chem. Soc.* **2009**, *131*, 1565−1574.

(6) (a) de Bruin, T.; Raybaud, P.; Toulhoat, H. *Organometallics* **2008**, *27*, 4864−4872. (b) Chisholm, M. H.; Gallucci, J. C.; Yaman, G. *Inorg. Chem.* **2007**, *46*, 8676−8683. (c) Zhang, A.; RajanBabu, T. V. *J. Am. Chem. Soc.* **2005**, *128*, 54−55. (d) Clarke, M. L.; Cole-Hamilton, D. J.; Foster, D. F.; Slawin, A. M. Z.; Woollins, J. D. *J. Chem. Soc., Dalton Trans.* **2002**, *8*, 1618−1624.

(7) (a) Bader, A.; Lindner, E. *Coord. Chem. Rev.* **1991**, *108*, 27−110. (b) Braunstein, P.; Naud, F. *Angew. Chem., Int. Ed.* **2001**, *40*, 680−699.

(8) Chapman, C. J.; Frost, C. G.; Mahon, M. F. *Dalton Trans.* **2006**, *18*, 2251−2262.

(9) (a) Li, J.; Tian, D.; Song, H.; Wang, C.; Zhu, X.; Cui, C.; Cheng, J. P. *Organometallics* **2008**, *27*, 1605−1611. (b) Brassat, I.; Keim, W.; Killat, S.; Möthrath, M.; Mastrorilli, P.; Nobile, C. F.; Suranna, G. P. *J. Mol. Catal. A: Chem.* **2000**, *157*, 41−58. (c) Mecking, S.; Keim, W. *Organometallics* **1996**, *15*, 2650−2656. (d) Britovsek, G. J. P.; Keim, W.; Mecking, S.; Sainz, D.; Wagner, T. *J. Chem. Soc. Chem. Commun.* **1993**, *21*, 1632−1634.

(10) (a) Popeney, C. S.; Rheingold, A. L.; Guan, Z. *Organometallics* **2009**, *28*, 4452−4463. (b) Leung, D. H.; Ziller, J. W.; Guan, Z. *J. Am. Chem. Soc.* **2008**, *130*, 7538−7539.

(11) (a) Wiedemann, T.; Voit, G.; Tchernook, A.; Roesle, P.; Göttker-Schnetmann, I.; Mecking, S. *J. Am. Chem. Soc.* **2014**, *136*, 2078−2085. (b) Ye, Z.; Xu, L.; Dong, Z.; Xiang, P. *Chem. Commun.* **2013**, *49*, 6235−6255. (c) Xiang, P.; Ye, Z.; Subramanian, R. *Polymer* **2011**, *52*, 5027−5039. (d) Morgan, S.; Ye, Z.; Subramanian, R.; Zhu, S. *Polym. Eng. Sci.* **2010**, *50*, 911−918. (e) Wang, J.; Kontopoulou, M.; Ye, Z.; Subramanian, R.; Zhu, S. *J. Rheol.* **2008**, *52*, 243−260.

(12) See the Supporting Information.

(13) (a) Seger, M. R.; Maciel, G. E. *Anal. Chem.* **2004**, *76*, 5734−5747. (b) Jurkiewicz, A.; Eilerts, N. W.; Hsieh, E. T. *Macromolecules* **1999**, *32*, 5471−5476. (c) Liu, W.; Ray, D. G.; Rinaldi, P. L. *Macromolecules* **1999**, *32*, 3817−3819.

(14) Izunobi, J. U.; Higginbotham, C. L. *J. Chem. Educ.* **2011**, *88*, 1098−1104.

(15) Average distances in the Cambridge Crystallographic Data Base (January 2014) are: Ni−$O_{phenol}$ = 1.904(2); Ni−$N_{imine}$ = 1.926(3); C−$O_{phenol}$ = 1.298(2); C═$N_{imine}$ = 1.296(2).

(16) Salata, M. R.; Marks, T. J. *Macromolecules* **2009**, *42*, 1920−1933.

(17) Guan, Z.; Cotts, P. M.; McCord, E. F.; McLain, S. J. *Science* **1999**, *283*, 2059−2062.

(18) Peng, K.; Xiao, S. *J. Mol. Catal.* **1994**, *90*, 201−211.

(19) (a) Hasanayn, F.; Achord, P.; Braunstein, P.; Magnier, H. J.; Krogh-Jespersen, K.; Goldman, A. S. *Organometallics* **2012**, *31*, 4680−4692. (b) Heyndrickx, W.; Occhipinti, G.; Minenkov, Y.; Jensen, V. R. *Chem.—Eur. J.* **2011**, *17*, 14628−14642.

(20) Soshnikov, I. E.; Semikolenova, N. V.; Zakharov, V. A.; Möller, H. M.; Ölscher, F.; Osichow, A.; Göttker-Schnettmann, I.; Mecking, S.; Talsi, E. P.; Bryliakov, K. P. *Chem. − Eur. J.* **2013**, *19*, 11409−11417.